APPLIED ORGANOMETALLIC CHEMISTRY
Appl. Organometal. Chem. 2006; **20**: 638–647
Published online 7 August 2006 in Wiley InterScience
(www.interscience.wiley.com) DOI:10.1002/aoc.1123

Shape-controlled synthesis of Pt nanocrystals: an evolution of the tetrahedral shape

Ying-Tao Yu and Bo-Qing Xu*

Innovative Catalysis Program, Key Laboratory of Organic Optoelectronics and Molecular Engineering, Department of Chemistry, Tsinghua University, Beijing 100084, People's Republic of China

Received 29 March 2006; Accepted 13 May 2006

Platinum nanocrystals with sizes smaller than 10 nm are obtained by H_2-reduction of aqueous K_2PtCl_6 in the presence of different concentrations of poly (*N*-vinyl-2-pyrrolidone; PVP : $M_w \approx 360\,000$) at pH = 2.5–7.0. Tetrahedral Pt nanocrystals (3–10 nm) are produced with high selectivity (73–83% by number) at moderate PVP : K_2PtCl_6 ratios. The co-existing round/spheroidal crystallites are found to be smaller than the tetrahedrally shaped ones in the systems of varying K_2PtCl_6 : PVP ratios. Careful examinations of the particle size and shape evolution of the crystallites at different stages of the crystal growth with transmission electron microscopy (TEM) and ultraviolet–visible absorption spectroscopy (UV–vis) suggest that the tetradedrally shaped Pt crystallites share the same type of nuclei with the round ones at the early stage of the crystal formation. Evolution of the tetrahedral shape happens in the later slow crystal growth. Copyright © 2006 John Wiley & Sons, Ltd.

KEYWORDS: platinum nanoparticles; tetradedral crystallite; crystal growth; *N*-vinyl-2-pyrrolidone; shape evolution; UV–vis spectroscopy

INTRODUCTION

Size- and shape-controlled syntheses of nano-sized metal and compounds are important both fundamentally and technically in the related nanotechnologies.[1–10] Platinum nanocrystals are important in thermo-,[11,12] photo-[13] and electrocatalysis,[14,15] in adsorption[16] and sensor technologies[17] and are also widely used in advanced optical,[18] electronic[19] and magnetic devices.[20] Differently shaped Pt nanocrystals have been synthesized with H_2 reduction of K_2PtCl_4 protected by sodium polyacrylate (NaPA : $M_w \approx 2100$),[1,21] or of H_2PtCl_6 by poly (*N*-vinyl-2-pyrrolidone; PVP : $M_w \approx 40\,000$).[22] In these earlier works, tetrahedral, truncated octahedral and cubic crystallites were observed to evolve simultaneously. Working with the system of K_2PtCl_4–NaPA, El-Sayed *et al*.[1,21] observed that small nanocrystals (<8 nm[1], <5 nm[21]) formed during the early stages of growth or at high protector concentration (K_2PtCl_4 : NaPA = 1 : 5) displayed distributions with a dominance of the tetrahedral shape. In the later stages of the growth or at low polymer concentration, the tetrahedrons were transformed into truncated octahedrons and eventually into cubes. They proposed that competition between the Pt^{2+} reduction and the polymer protection on the different nanoparticle surfaces was crucial in controlling the final shape-selectivity of the nanocrystals.[21] Thereafter, 'tetrahedral nuclei' were proposed by Teranishi *et al*.[22] to account for the formation of tetrahedral crystallites from the reduction of H_2PtCl_6–poly (*N*-vinyl-2-pyrrolidone; PVP : $M_w \approx 40\,000$).[22] However, when poly(*N*-isopropylacrylamide)[23] or oxalate[24] was used as the protector, cubic Pt crystallites (7–12 nm) were selectively formed, but tetrahedral crystallites were hardly detected during the growth stage. Also, we found recently that the result of the synthesis with K_2PtCl_4–NaPA was difficult to reproduce due to rapid hydrolysis of the Pt(II)–precursor (K_2PtCl_4) in aqueous solution.[25] With fresh K_2PtCl_4–NaPA solution in the dark, we produced Pt nanocrystals (4–17 nm) consisting of cubic (25–30%) and round or truncated polyhedral (ca. 70%) shapes. Similar synthesis with fresh K_2PtCl_6–NaPA selectively produced truncated octahedral crystallites (3–15 nm),[25] which is at variance with Teranishi *et al*., who produced a condiderable amount of tetrahedrons.[22] These works seem to suggest that the mechanism and kinetics leading to the shape-controlled synthesis of Pt nanocrystals can be affected not only by the

*Correspondence to: Bo-Qing Xu, Innovative Catalysis Program, Key Lab of Organic Optoelectronics & Molecular Engineering, Department of Chemistry, Tsinghua University, Beijing 100084, People's Republic of China.
E-mail: bqxu@tsinghua.edu.cn
Contract/grant sponsor: National Natural Science foundation of China; Contract/grant numbers: 20125310; 20573062.

state of Pt precursor but also by the nature of the protector molecules (El-Sayed MA, personal communications).[26]

The shape-selective synthesis of Pt nanocrystals is attempted in the present work by using K_2PtCl_6 for the Pt precursor and PVP for the protector. We choose K_2PtCl_6 for the precursor of Pt because the synthesis with K_2PtCl_4–NaPA solution was severely affected by the rapid hydrolysis and the products were obtained with poor reproducibility (El-Sayed MA, personal communications).[25] TEM analysis of the metal colloids and UV–vis absorption of the colloid solution were employed to monitor the evolution of the tetrahedrons during the syntheses with varying K_2PtCl_6 : PVP ratios.[27] The results suggest that the initial shape of the crystallite nuclei is round and the evolution of the tetrahedral shape proceeds in the later slow crystal growth.

EXPERIMENTAL

Pyrex tubular reactor (ca. 20 ml) with freshly prepared aqueous solutions (pH = 3.1–4.5) of K_2PtCl_6 ($2.0–5.0 \times 10^{-4}$ M) and PVP (0.2–5.0 g/l, $M_w \approx 360\,000$) were purged at room temperature with bubbling argon (80 ml/min) for 20 min. The reagents K_2PtCl_6 (AR) and PVP ($M_w \approx 360\,000$) were purchased from Beijing Chemicals Co. and Aldrich, respectively. The bubbling gas was then switched to an H_2 flow (100 ml/min) for 45 min and the reactor was then sealed off under ambient hydrogen. After standing for 24 h from the sealing, the reactor was opened and the Pt colloids were sampled and loaded on carbon-coated Cu grids for TEM (JEM-200CX; 200 kV) measurements. The reactor was wrapped with aluminum foil to protect the solution from exposure to surrounding light in the entire period of the synthesis. In some experiments, the pH of the initial solution containing 2.0×10^{-4} M K_2PtCl_6 and 1 g/l PVP was changed to pH ≈ 2.5 with dilute HCl and to pH ≈ 7.0 with dilute KOH.

HRTEM and energy dispersive spectroscopy (EDS) measurements were performed using a JEM-2010F (200 kV) instrument equipped with a Link ISIS-300 probe. UV–vis spectra were taken on a Shimadzu UV-2100 spectrometer. The back-scattered electron images were obtained on a JSM 6301 SEM instrument. Confocal Raman spectra were taken on a Renishaw 1000 Raman spectrometer working with He–Ne laser irradiation (633 nm) at a power of 2.25 mW.

RESULTS AND DISCUSSION

Shape-selectivity of Pt crystallites

Figure 1 shows the crystallite morphology produced by H_2 reduction of K_2PtCl_6 (2.0×10^{-4} M) in the absence and presence of varying amount of PVP. The column graphs located on the right of the TEM photos show the size distributions and the sizes appearing in the graphs give the average sizes of the Pt crystallites. A total number of ca. 220 nanocrystals was measured in the determination of the crystallite size distribution in each of the samples. In the absence of a PVP protector, the reduction of aqueous K_2PtCl_6 produced round or irregularly shaped particles (5–15 nm) together with some fibre-like (ca. 4 × 50 nm) ones [Fig. 1(A)]. In the contrast, tetrahedral Pt crystallites with sizes of 3–10 nm were obtained in fairly high percentages (ca. 80%) by number in the syntheses at PVP concentrations of 0.2 g/l [Fig. 1(B)] and 1.0 g/l [Fig. 1(C)]. Some smaller crystallites (<3 nm) were also observed in Fig. 1(B) and (C), but they were generally in round shapes. Here, the 'round' shapes refer to those truncated polyhedrons that are closer to spheroids than truncated octahedrons (some magnified round crystallites are shown later in Fig. 6). When the concentration of PVP was increased to 5.0 g/l [Fig. 1(D)], the obtained colloids became dominated by small round crystallites (2–4 nm) with less than 5% tetrahedrons.

We changed the pH of the initial solution containing 2.0×10^{-4} M K_2PtCl_6 and 1 g/l PVP at pH ≈ 4.0 to pH ≈ 2.5 with dilute HCl and to pH ≈ 7.0 with KOH to investigate the effect of pH on the formation of tetrahedral crystallites. The change in pH produced small differences in the shape-selectivity of the synthesized Pt nanocrystals; the selectivity of tetrahedral nanocrystallites was 76% at pH = 2.5 and 73% at pH = 7.0, slightly lower than that (83%) at pH = 4.0 [Fig. 1(C)].

Shown in Fig. 2 are representatives of high-resolution TEM images of the tetrahedral Pt crystallites. The image located on the top-left of this figure reveals a tetrahedral Pt crystallite that partly overlaps with one of the smaller round crystallites; the energy dispersive spectrum (EDS) of this selected area (not shown) confirmed that the particles are indeed crystallites of Pt. Some high-resolution images enabled us to measure the fringe spacing, which verified that the projected triangular surfaces belong to the {111} facet of crystallite Pt. Also, the presence of the fourth corner in a tetrahedral crystallite was observed by a tilting operation attempted in TEM measurements.[27]

The shape evolution feature of Pt crystallites became evident in Fig. 3, when the synthesis was made with a solution containing much higher concentration of K_2PtCl_6 (5.0×10^{-4} M), but the protector concentration was kept the same as in Fig. 1(C) (1.0 g/l PVP). This specific case enabled more overlapping of the nucleation and crystal growth, which led to much broader size distribution (2–15 nm) and allowed a direct observation within the same TEM image of Pt crystallites at different 'growth-time' from their nucleation (Fig. 3). In general, the sizes of the tetrahedral crystallites are considerably bigger than those of the round ones,[27] which seems difficult to explain with the earlier assumption that 'tetrahedral nuclei' were formed at the initial stages of the crystal growth.[21,22]

Although it is very difficult to define the exact physical size of a crystal nucleus and it is extremely difficult to detect how a stable crystal nucleus is formed,[28] the above data seem to indicate that the 'crystal nuclei' are

DOI: 10.1002/aoc

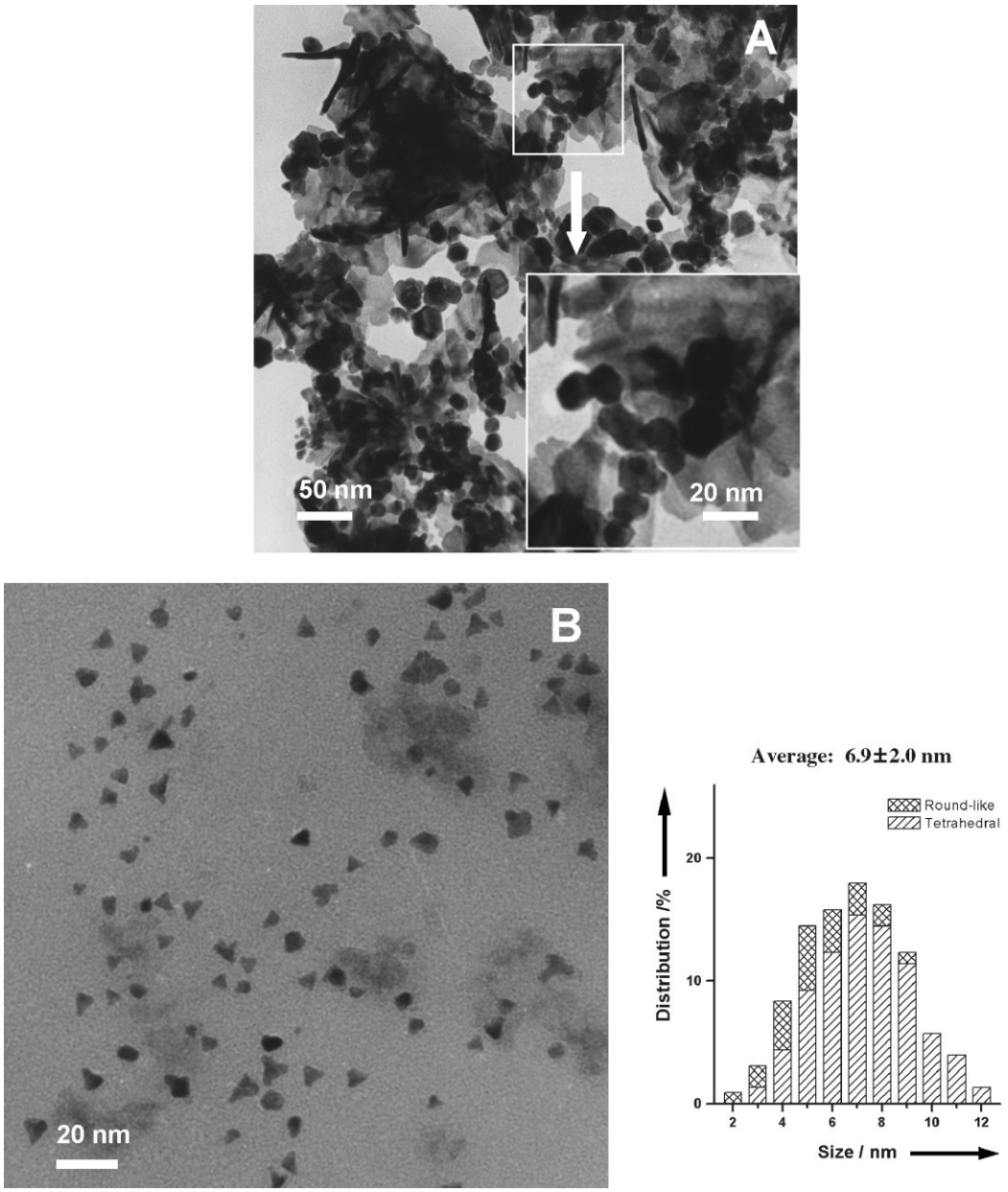

Figure 1. TEM images of Pt nanocrystals produced by H_2 reduction of K_2PtCl_6 (2.0×10^{-4} M) solutions containing 0 (A), 0.2 (B), 1.0 (C) and 5.0 g/l (D) PVP, respectively. The column graphs on the right of each TEM photos were obtained by measuring 228 (B), 207 (C) and 217 crystallites (D), respectively.

generated as 'round' objects and then develop pronounced {111} faceting by inhibition of growth on the other sets of crystal faces. Because of the difference in lattice density and surface energy, the growth rates of Pt facets with different indexes differ from each other. According to the overlapping growth model, the faster growing facets often disappear and the crystallite eventually develops a special shape enclosed with slow-growing ones.[27] Since protector polymer is required for the shape-selective synthesis of Pt nanocrystals[1,21–23,26,27] and our synthesis in the absence of PVP polymer produced no tetrahedron but round and irregularly shaped crystals [Fig. 1(A)], protection of the {111} facets by PVP polymer is believed to be crucial for the evolution of the tetrahedral shape. We believe that chemical adsorptions on Pt surface of PVP molecules could be responsible for the shape evolution. To gain insight into the PVP–Pt interaction, part (5 ml) of the solution containing the nanocrystals shown in Fig. 1(C) was first concentrated by water evaporation and then loaded onto a glass (5×5 mm) slide to make a dry film of the PVP–Pt nanocrystals. Shown in Fig. 4(A) are the back-scattered electron images of the film in the SEM mode. Since the element platinum is far

DOI: 10.1002/aoc

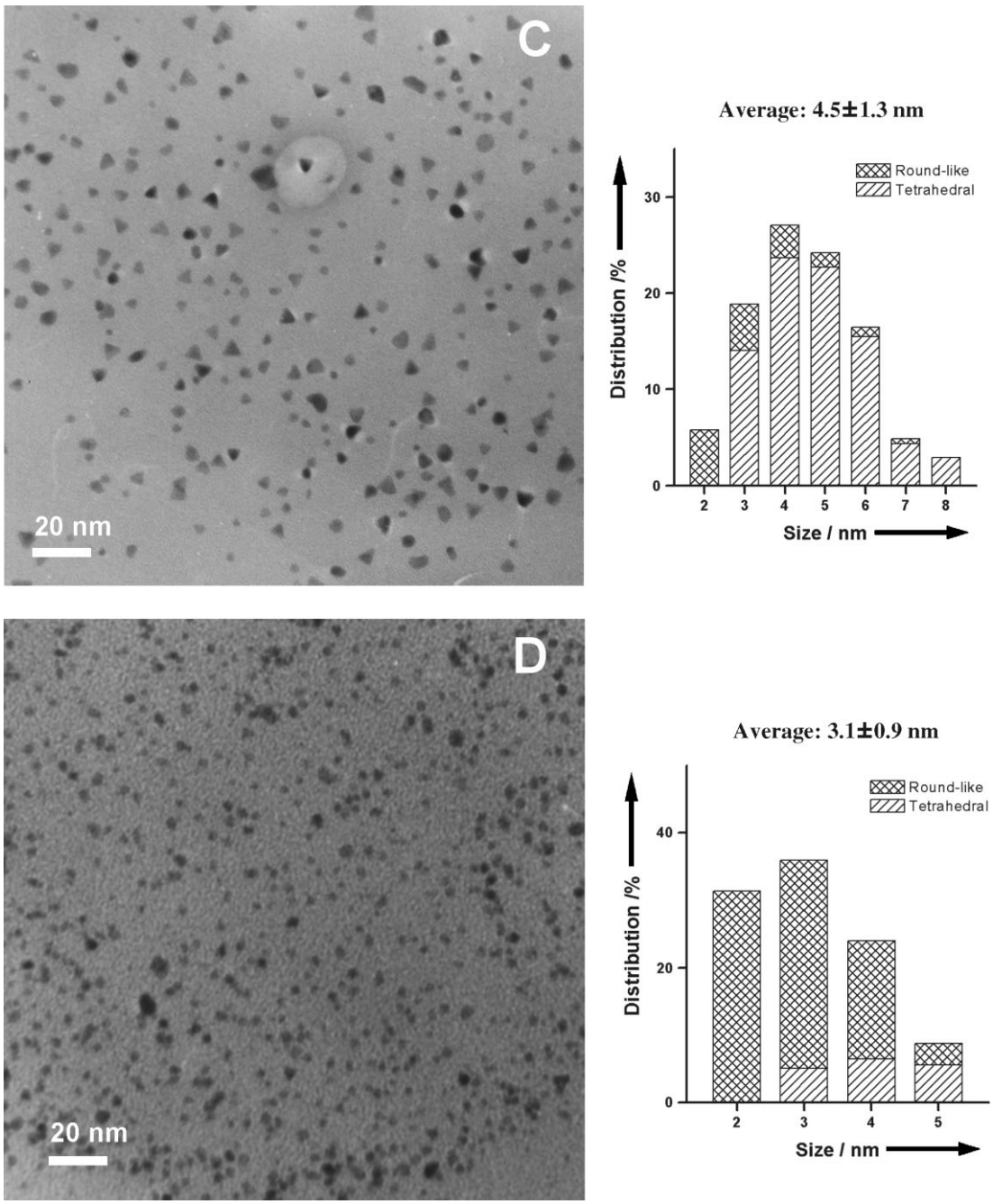

Figure 1. (*Continued*).

heavier than all the other elements in the sample, the bright white spots probably represent a rough image of the Pt crystallites. In fact, one of the big spots marked in Fig. 4(A) was confirmed to be Pt by selected area EDS identification. Thus, the separated spots indicate that Pt nanocrystals in the film are well dispersed, which agrees with Fig. 1(C) of the TEM observation. Figure 4(B) is the confocal laser Raman spectrum covering an area of ca. 4 μm diameter. It is seen that the C═O stretching frequency [$\nu_{(C=O)} = 1675\ cm^{-1}$] of PVP associated with Pt colloids is significantly higher than the $\nu_{(C=O)}$ (1662 cm^{-1}) in 'free' PVP. This strengthening of the C═O bond is taken as a strong evidence for the existence of chemical adsorption of PVP on Pt colloids.

It is likely that the adsorption of PVP prefers {111} to the other facets. When the PVP PVP : K_2PtCl_6 ratio is higher than that required for protecting all of the {111} facets, PVP adsorption on the other facets can be inevitable and the formation of tetrahedral crystallites can be difficult, resulting in the production of small crystallites with non-tetrahedral

DOI: 10.1002/aoc

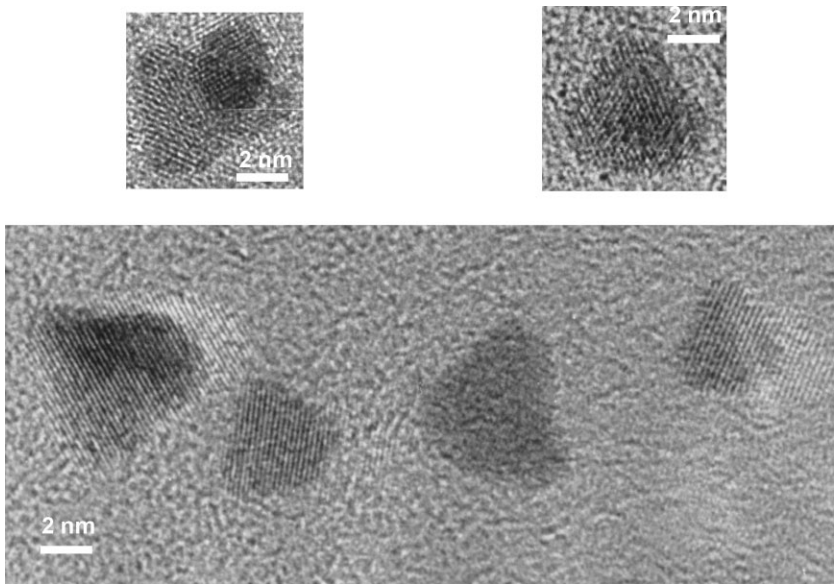

Figure 2. High-resolution TEM images of some tetrahedral Pt nanocrystals produced by H_2 reduction of K_2PtCl_6 (2.0×10^{-4} M) solutions containing 1.0 g/l PVP.

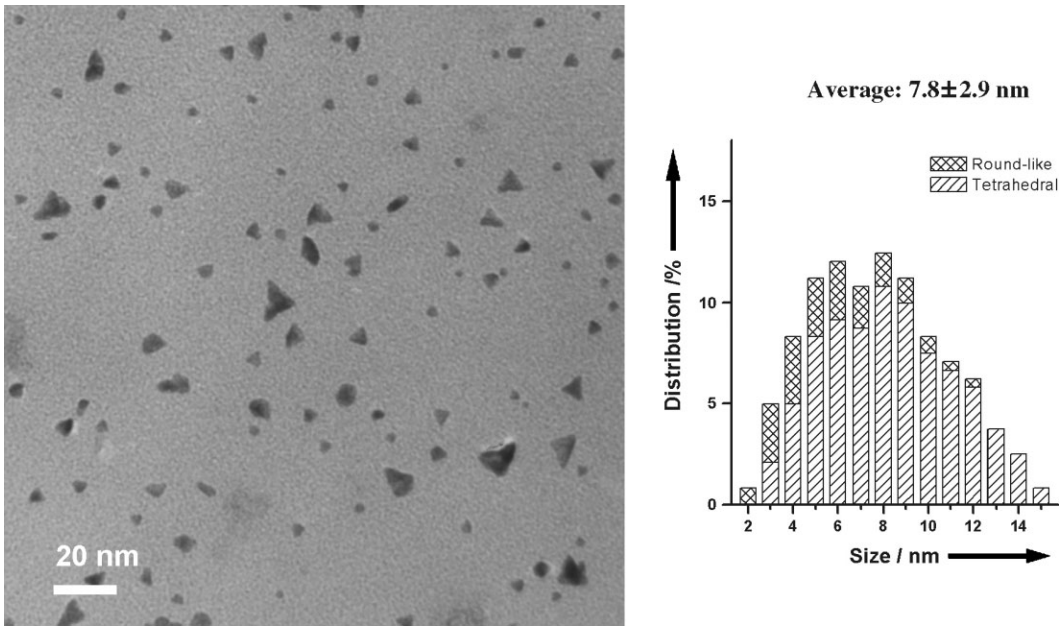

Figure 3. TEM images of Pt nanocrystals produced by H_2 reduction of K_2PtCl_6 (5.0×10^{-4} M) solution in the presence of 1.0 g/l PVP. The column graph was obtained by measuring 241 particles.

shapes [Fig. 1(D)]. On the other hand, a lower PVP : K_2PtCl_6 ratio will cause insufficient protection of the {111} facets, which would lead to nanocrystals being protected to different degrees and having varying periods of the crystallite growth (Fig. 3). Some nanocrystals with transition shapes in between the tetrahedron and tetrapod were detected in Figs 1(B) and 3. The formation of the transition shapes may imply that at some lower PVP : K_2PtCl_6 ratios, the protection of PVP can remain efficient for the middle part of the {111} facets, but not as such for the edges or corners. Scheme 1 gives a sketch of the dependence of shape evolution on the PVP : K_2PtCl_6 ratio.

Evolution of the tetrahedral shape in slow crystal growth

The formation of Pt colloids was characterized by UV–vis spectroscopy that monitors the consequence of H_2 reduction

DOI: 10.1002/aoc

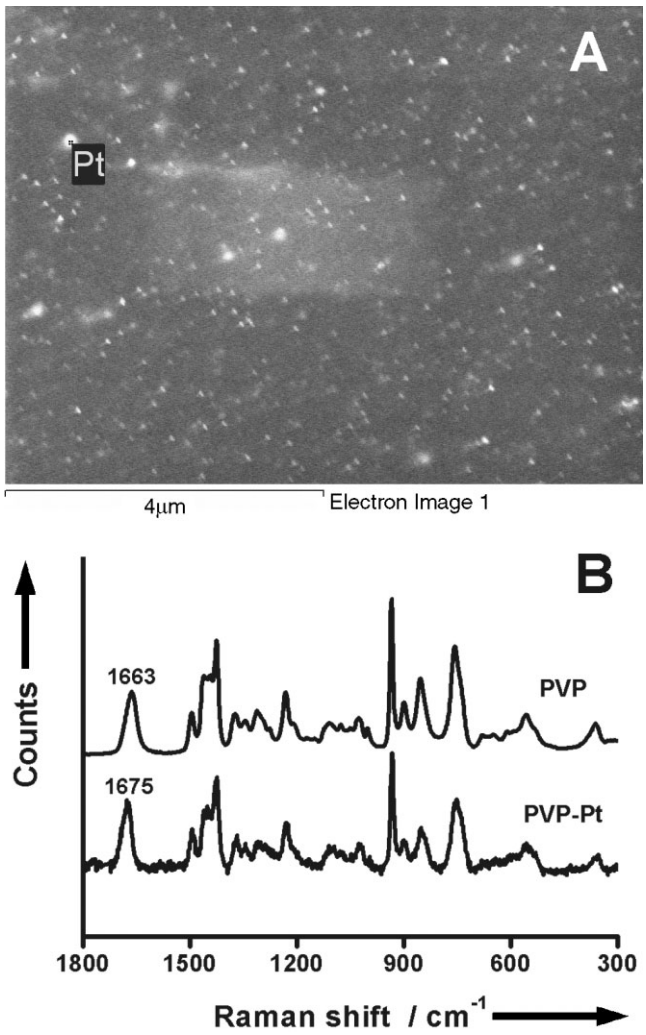

Figure 4. (A) Back-scattered electron images in SEM mode of the PVP-associated Pt colloids obtained from H_2 reduction of K_2PtCl_6 (2.0×10^{-4} M) solution in the presence of 1.0 g/l PVP. (B) Raman spectra of 'free' PVP and PVP associated with Pt colloids.

of K_2PtCl_6 (2.0×10^{-4} M) protected by PVP (1.0 g/l) in a bulky reactor (ca.100 ml); the results are given in Fig. 5. The UV–vis spectrum of metal colloids contains usually two components, one from the true absorptions and the other from light scattering of the colloid particles. According to Kreibig,[29,30] the component from the scattering will become less significant with reducing the colloid particle size and its contribution in the spectrum can be ignored when the colloid particles are smaller than 10 nm. Since the Pt nanocrystals are sufficiently protected and separated from growing bigger than 10 nm in the system under examination (Fig. 6), it is possible to use the UV–vis spectra in Fig. 5 to evaluate the true absorptions of the Pt nanocrystals during the crystal growth. The characteristic absorption of $[PtCl_6]^{2-}$ ions at ca. 263 nm in Fig. 5(A) decreased rapidly during the 45 min bubbling of H_2. However, the very week absorptions at wavelength longer than 350 nm [spectra a, b and c in Fig. 5(A)] indicate that the formation of Pt colloids is not significant during this period of H_2 reduction since Pt colloids in aqueous solution are expected to show absorptions peaking at ca. 215 nm and tailing to 800 nm.[31] Although the absorptions of Pt colloids might overlap significantly with the absorptions of PVP, $[PtCl_6]^{2-}$ and other intermediate Pt-containing ions below 350 nm, the spectra at longer wavelength (350–800 nm) are little affected [Fig. 5(A)] and can be mainly attributed to 'pure' absorptions of the Pt colloids. This argument was supported by our frequent detection of possible colloid formation with TEM, which showed little formation of regular Pt particles within the 45 min period of H_2 bubbling.

The 'pure' absorptions of Pt colloids (350–800 nm) were intensified remarkably in the first 4 h after the termination of H_2 bubbling and the intensification became less pronounced at longer times [spectra d–h and h in Fig. 5(A)]. According to Henglein,[32] the coalescence of metal atoms in solution leads first to subnanometer clusters and then nanocrystals. For a constant number of metal atoms, the absorption coefficient per metal atom increases with increasing the aggregate size at the beginning and then becomes independent of the particle size when the number of atoms in an aggregate exceeds a certain value (n_m) and when the particle size is smaller than 20 nm.[29–33] This principle was supported by the observation that the absorption of well-separated particles with sizes ranging from ca. 3 to 20 nm was proportional to the total number of metal atoms in all the crystallites but little affected by the sizes of the crystallites.[32] In practice, the sub-nanometer clusters containing less than n_m metal atoms are generally short-lived,[28] and the number n_m can be much smaller than the number of atoms in an aggregate of 3 nm, e.g. $n_m = 12$ for Ag.[34] Thus, the contribution from the subnanometer clusters should be small in the UV–vis absorptions and the absorption

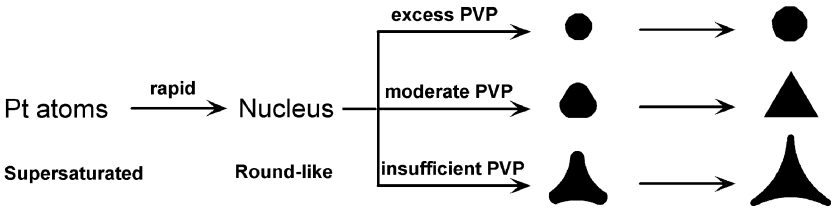

Scheme 1. Shape evolution of Pt nanocrystal at different K_2PtCl_6–PVP ratios.

DOI: 10.1002/aoc

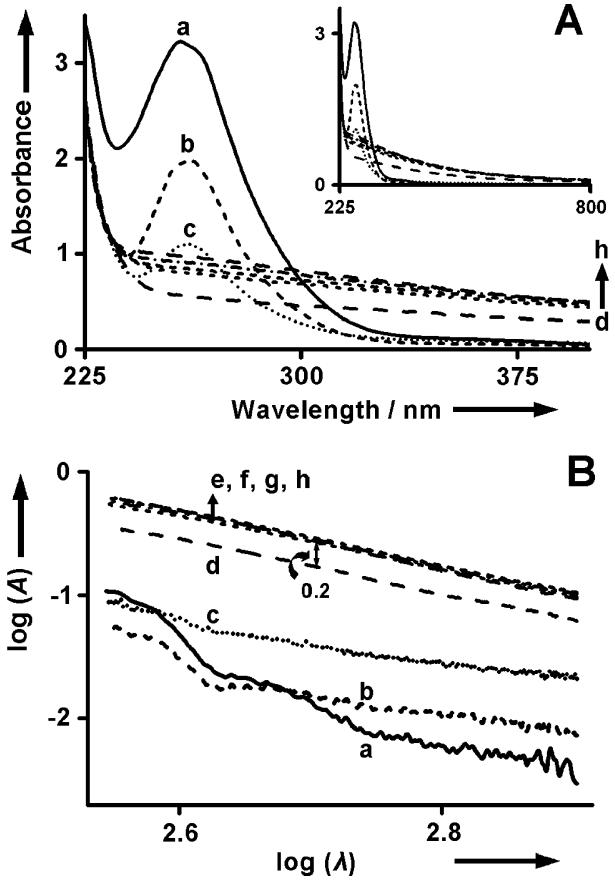

Figure 5. (A) UV–vis spectra of Pt nanocrystals in solution. The solution of K_2PtCl_6 (2.0×10^{-4} M) and PVP (1.0 g/l) was purged with Ar for 20 min (a), followed by bubbling H_2 for 15min (b) and 45 min (c). Spectra from d to h were obtained after sealing for 2, 4, 6, 9 and 52 h, respectively. (B) Log(A)–log(λ) curves of UV–vis spectra between 350 and 800 nm.

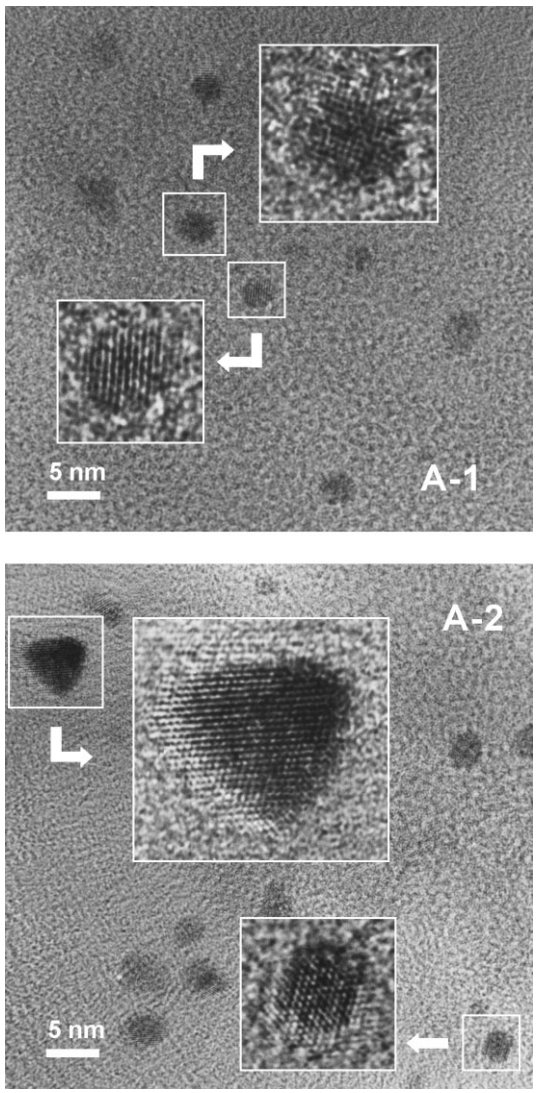

Figure 6. TEM images of Pt nanocrystals after standing for 2 (A-1, A-2), 4 (B), 9 (C), 13 (D) and 52 h (E) of the sealed reactor; the HRTEM insets in the A-photos show the round shape of small Pt crystals at the early stages of the crystal growth. Before the sealing, the initial solution containing 2.0×10^{-4} M K_2PtCl_6 and 1.0 g/l PVP was bubbled with Ar for 20 min and then H_2 for 45 min. The column graphs were obtained, respectively, by measuring 202 (A), 219 (B), 235 (C), 205 (D) and 261 particles (E). Figure 6(F) shows the time-dependent selectivity of tetrahedral crystallites obtained by measuring 200–300 panticles for every sample.

increase in the range 350–800 nm can be mainly attributed to the increased Pt atoms in the nanocrystals. The 'pure' absorptions of Pt colloids are expressed in terms of a double-logarithmic curve, log(A) – log(λ), in Fig. 5(B). Since the slope of log(A) – log(λ) is closely related to the aggregagtion state of the nanocrystals in solution,[35,36] the hardly changed curve slope during the period 2–52 h standing after the stop of H_2 bubbling indicates that Pt nanocrystals grown to these stages in the solution are well separated or less interacting. These similar curve slopes also suggest that the change in crystallite shape or the evolution of tetrahedrons during the later crystal growth (see also Fig. 6) has little effect on the absorption coefficient of Pt atoms in the crystallites.

Very weak absorptions at 350–800 nm before and during the reduction with bubbling H_2 [Fig. 5(A)] were characterized by the very negative log(A) values for curves a–c in Fig. 5(B). Although the absolute values of the absorptions [spectra a–c in Fig. 5(A)] were negligible in comparison with those when larger number of Pt nanocrystals were formed [spectra d–h in Fig. 5(A)], it is noticeable that the curves obtained at these earlier stages of incomplete reduction of the $[PtCl_6]^{2-}$ ions show significantly different slopes from those at ≥2 h after the termination of H_2 bubbling. The difference in slopes of curves a–c reflects a variation in the aggregation state of the very small colloid particles in the solution[32,33,36] and suggests to a gradual transition into the growth of Pt nanocrystals

DOI: 10.1002/aoc

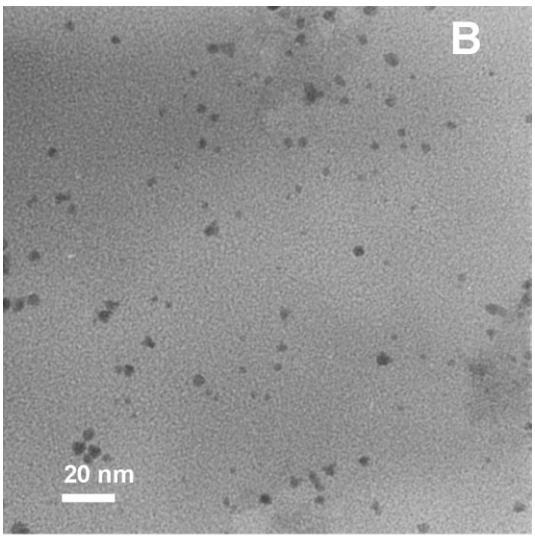

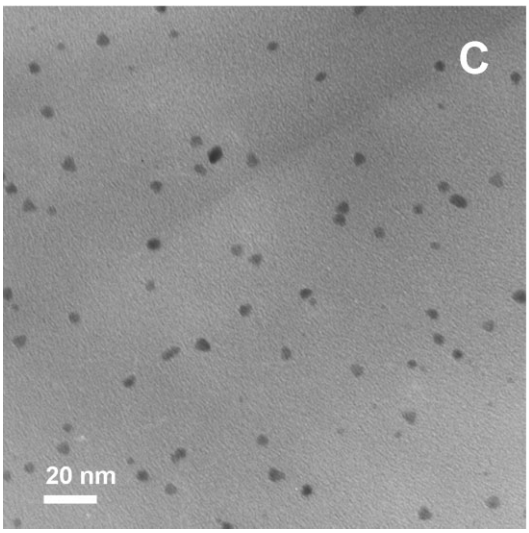

Figure 6. (*Continued*).

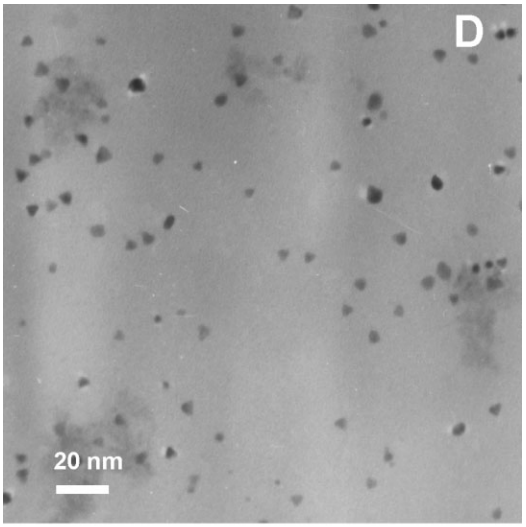

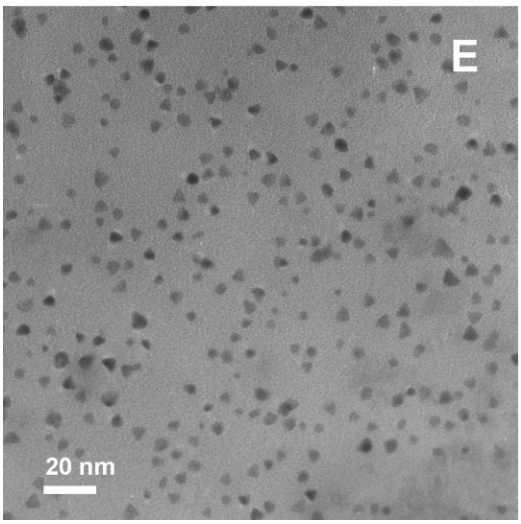

Figure 6. (*Continued*).

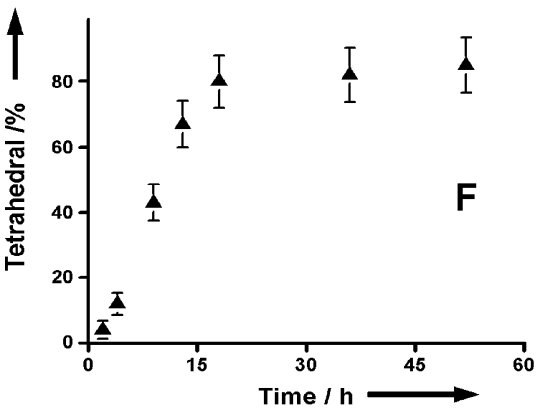

Figure 6. (*Continued*).

from a relatively rapid reduction of the $[PtCl_6]^{2-}$ ions and formation of subnanometer Pt clusters with varying cluster sizes.

It is interesting that the vertical distance between the curves decreased dramatically with the standing time after the termination of H_2 bubbling [Fig. 5(B) curves c–h]. The remarkable difference in slope for curves c and d together with a large vertical distance between these two curves, which were measured at 0 and 2 hrs after the termination of H_2 bubbling, would mean that very rapid crystallization, including nucleus formation and growth to small (2–4 nm) crystallites [see also Fig. 6(A)], happens during this early stage. The significant distance (ca. 0.2) between the curves measured at 2 h and those at times longer than 4 h after the stop of H_2 bubbling suggests that the majority of Pt nanocrystals during the synthesis were formed in the first 4 h after the termination of H_2 bubbling. According to Lambert–Beer's law, the absorption, A, is proportional to the concentration, C. At a given wavelength, the following

DOI: 10.1002/aoc

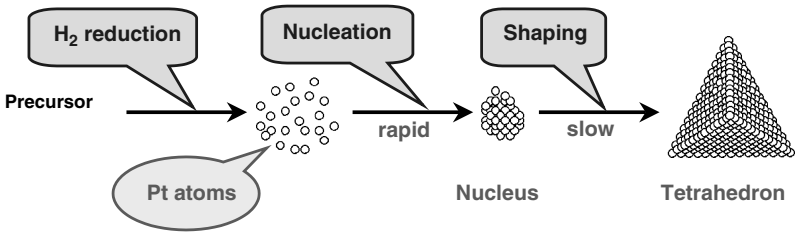

Scheme 2. Evolution toward tetrahedron in slow growth of Pt nanocrystals..

calculation can be performed to evaluate the difference in overall concentration of the Pt nanocrystals during a certain period in the crystal growth, e.g., $d_{4-2h} = \log(A_{4h}) - \log(A_{2h}) = \log(A_{4h}/A_{2h}) = \log(C_{4h}/C_{2h})$, where the subscripts denote the standing time after the termination of H_2 bubbling, and d_{4-2h} measures the vertical distance (ca. 0.2) between the $\log(A) - \log(\lambda)$ curves at 2 and 4 h after the termination of H_2 bubbling. Thus, the overall concentration of Pt nanocrystals at 2 h was ca. 63% (i.e. $C_{2h}/C_{4h} \approx 10^{-0.2} \approx 63\%$) of that at 4 h after the termination of H_2 bubbling. Only slight changes of the absorption occurred after the 4 h, suggesting that the growth of Pt nanocrystals become much slower thereafter. Since the absorption of Pt colloids was small during the 45 min of bubbling H_2, the formation of Pt nuclei and the growth of crystallites could be rapid and proceeded simultaneously in the first 2 h after the termination of H_2 bubbling. At longer times, slow crystallite growth became dominant and the formation of new crystallites hardly occurred.

All of the samples showing the UV–vis spectra of Fig. 5 were examined with TEM/HRTEM. No crystallite formation was detected during the 45 min H_2 bubbling but small round crystallites (ca. 2–3 nm) were observed to dominate the sample at 2 h after the termination of H_2 bubbling [Fig. 6(A)], when the overall concentration of Pt crystallites increased rapidly. The tetrahedral crystallites detected were less than 5% by number of the round ones but they were clearly bigger [4–8 nm, Fig. 6(A-2)] than the majority of the round counterparts. The possibility of detecting tetrahedrally shaped nanocrystals increased to 10–15% at 4 h [Fig. 6(B)], 30–50% at 9 h [Fig. 6(C)], and 80–90% at times longer than 20 h [Fig. 6(D, E)] after the termination of H_2 bubbling. Apparently, the percentage of the tetrahedral crystallites increased steadily, as shown in Fig. 6(F), with the 'standing time' after the termination of H_2 bubbling, when the crystal growth or increase in the overall concentration of Pt nanocrystals became very slow. These results suggest that evolution of tetrahedral crystallites occurs mainly in the slow crystal growth.[27] The difficulty in developing the tetrahedral shape at the early stage of the crystal growth hints that the protection of PVP molecules for emerging {111} facets on very small 'nuclei' (<3.0 nm) was not effective in the rapid growth, which agrees with Teranishi *et al*., who produced truncated octahedral Pt crystallites with rapid methanol reduction of $PtCl_6^{2-}$ ions in the presence of PVP ($M_w \approx 40\,000$).[22] With rapid hydrogen reduction of K_2PtCl_4–NaPA, El-Sayed *et al*. also produced only round particles (El-Sayed MA, personal communications). The protected Pt {111} facets turn into the slowest growing ones that induce the shaping toward tetrahedrons. This model for the tetrahedron evolution is shown in Scheme 2.

Very recently, a communication by Xia *et al*. also showed that, in polyol synthesis of Pt nanoparticles, the addition of enough sodium nitrate can greatly slow down the reduction of Pt(IV) and Pt(II) precursors by ethylene glycol and induce the formation of larger tetrahedral and octahedral Pt nanocrystallites with well-defined facets from irregular Pt spheroids with rounded profiles.[37]

CONCLUSIONS

The ratio of K_2PtCl_6 : PVP significantly affects the shape-controlled synthesis of Pt nanocrystals. The present examinations with TEM and UV–vis spectrometry into the synthesis with proper K_2PtCl_6 : PVP ratio suggest no formation of tetrahedral but round objects at the early stage of the crystallization. Formation of tetrahedral Pt crystallites from the small round objects takes place during the later external facet evolution in slow growth. Further work is needed to explore if the present observation of shape evolution can be extended to other systems of crystallite formation with different metal precursors and protector or capping molecules.

Acknowledgments

The high-resolution TEM images were obtained with the kind help of Dr Xi-Hua Chen at the Center of Electron Microscopy, School of Materials Science and Engineering, Tsinghua University. We acknowledge the financial support of this work from NSF of China (grant nos 20590362 and 20573062). We thank also the Analytic Funding of Tsinghua University for partial support of the TEM measurements.

REFERENCES

1. Ahamadi TS, Wang ZL, Green TC, Henglein A, El-Sayed MA. *Science* 1996; **272**: 1924.
2. Bradley JS, Tesche B, Busser W, Maase M, Reetz MT. *J. Am. Chem. Soc.* 2000; **112**: 4631.
3. Sun Y, Xia Y. *Science*, 2002; **298**: 2176.

DOI: 10.1002/aoc

4. Puntes VF, Krishnan KM, Alivisatos AP. *Science* 2001; **291**: 2115.
5. Jin R, Cao Y, Mirkin CA, Kelly KL, Schatz GC, Zheng JG. *Science* 2001; **294**: 1901.
6. Jana NR, Gearheart L, Murphy CJ. *Adv. Mater.* 2001; **13**: 1389.
7. Filankembo A, Pileni MP. *Appl. Surf. Sci.* 2000; **164**: 260.
8. Jana NR, Wang ZL, Sau TK, Pal T. *Curr. Sci. (India)* 2000; **79**: 1367.
9. Selven ST, Hayakaw Ta, Nogami M, Möller M. *J. Phys. Chem. B* 1999; **103**: 744.
10. Yu Y, Chang S, Lee C, Wang CRC. *J. Phys. Chem. B* 1997; **101**: 6661.
11. Roucoux A, Schulz J, Patin H. *Chem. Rev.* 2002; **102**: 3757.
12. Balint I, Miyazaki A, Aika K. *Phys. Chem. Chem. Phys.* 2004; **6**: 2000.
13. Amouyal E, Koffi P. *J. Photochem.* 1985; **29**: 227.
14. Lewis LN. *Chem. Rev.* 1993; **93**: 2693.
15. Vidal-Iglesia FJ, Solla-Gullon J, Rodriguez P, Herrero E, Montiel V, Feliu JM, Aldaz A. *Electrochem. Commun.* 2004; **6**: 1080.
16. Somorjai GA. *Chem. Rev.* 1996; **96**: 1223.
17. Hibino T, Hashimato A, Mori K, Sano M. *Eletrochem. Solid St.* 2001; **4**: H9.
18. Fieldler S, Shirley SG, Schnelle T, Fuhr G. *Anal. Chem.* 1978; **70**: 1909.
19. Bogdanovskaya VA, Evstefeeva YE, Tarasevich MR, Galitskaya LN, Galitskii AB. *Russ. J. Electrochem.* 1997; **33**: 137.
20. Sun S, Anders S, Hamann HF, Thiele J, Baglin JEE, Thomson T, Fullerton EE, Murry CB, Terris BD. *J. Am. Chem. Soc.* 2002; **124**: 2884.
21. Petroski JM, Wang ZL, Green TC, El-Sayed MA. *J. Phys. Chem. B* 1998; **102**: 3316.
22. Teranishi T, Kurita R, Miyake M. *J. Inorg. Organometall. Polym.* 2000; **3**: 145.
23. Miyazaki A, Nakano Y. *Langmuir* 2000; **16**: 7109.
24. Fu X, Wang Y, Wu N Gui L, Tang Y. *Langmuir* 2002; **18**: 4619.
25. Yu YT, Xu BQ. *Acta Chim. Sin.* 2003; **61**: 1758.
26. Yu YT, Xu BQ. *Chem. J. Chin. Univ.* 2004; **25**: 2384.
27. Yu YT, Xu BQ. *Chin. Sci. Bull.* 2003; **48**: 2589.
28. Mullin JW. *Crystallization*, 3rd edn. Butterworth-Heinemann: Oxford, 1993; 172–288.
29. Kreibig U. *J. Phys. F* 1974; **4**: 999.
30. Kreibig U, Schmidt B, Breuer HD. *Phys. Rev. B* 1987; **36**: 5027.
31. Creighton JA, Eadon DG. *J. Chem. Soc. Fraday Trans.* 1991; **87**: 3881.
32. Henglein A. *J. Phys. Chem.* 1993; **97**: 5457.
33. Kreibig U, Genzel L. *Surf. Sci.* 1985; **156**: 678.
34. Henglein A, Tausch-Treml R. *J. Colloid Interface Sci.* 1981; **80**: 84.
35. Furlong DN, Launikonis AL, Sasse WHF. *J. Chem. Soc. Faraday Trans. 1* 1984; **80**: 571.
36. Henglein A, Ershov BG, Malowl M. *J. Phys. Chem.* 1995; **99**: 14129.
37. Herricks T, Chen JY, Xia YN. *Nano Lett.* 2004; **4**: 2367.

DOI: 10.1002/aoc